RSC Advances

ROYAL SOCIETY OF CHEMISTRY

www.rsc.org/advances

Theoretical prediction of low-density nanoporous frameworks of zinc sulfide based on Zn_nS_n (n=12, 16) nanocaged clusters

Yongliang Yong[1, 2, *], Xiaohong Li[1], Xiping Hao[1], Jingxiao Cao[1], and Tongwei Li[1]

[1] College of Physics and Engineering, Henan University of Science and Technology, Luoyang 471003, People's Republic of China

[2] Department of Physics, Zhejiang University, Hangzhou 310027, People's Republic of China

ABSTRACT

Using density functional theory calculations, the possibility of the formation of different low-density framework materials based on highly stable Zn_nS_n (n=12, 16) clusters is systematically investigated. Our cluster building blocks, which have high symmetries and large HOMO-LUMO gaps, are predicted to be strongly energetically preferred. Via the coalescence of Zn_nS_n (n=12, 16) building blocks, many kinds of low-density ZnS framework materials of varying porosity are thus proposed. All the frameworks differ from known synthesized materials and are predicted to be energetically stable at room temperature. These new materials are found to be semiconductors with wide bandgaps, indicating that they may have a promise for optoelectronic applications. Because of their nanoporous structure, they could be used for gas storage, heterogeneous catalysis, and filtration and so on. The insights we obtained here will be helpful for extending the range of properties and applications of ZnS materials.

Keywords: ZnS clusters, cluster-assembled materials, nanoporous frameworks, electronic properties, first-principles calculation

* Author to whom correspondence should be addressed. Electronic mail: ylyong@haust.edu.cn

1. Introduction

Since the discovery of the excellent properties and applications of aluminosilicate zeolites in the areas of ion-exchange, separations, and catalysis [1-3], the area of inorganic open-framework materials has become one of intense research activity. One of the objectives of the research into open-framework materials is to find materials possessing channels and other features that make them porous or nanoporous. These porous materials play an important role in many technologies related to energy and sustainability, such as catalysis, gas separation, water purification, and batteries [4-11]. In addition, in the current search for new and interesting nanoporous open-frameworks, the predictability of the framework architecture and the control of its dimensionality are essential, even if one is confronted with the underlying issue of polymorphism [12].

On the other hand, the prediction of the structures and properties of new materials from first principles is an important issue in fields as diverse as materials science and pharmacology, since it can be guide synthetic work efficiently towards the formulation of new materials with useful and novel properties, and is a great complementary tool to experimental polymorph screening. There are a number of diverse promising approaches to be used for the prediction of crystal structures, as outlined in a recent comprehensive review by Woodley and Catlow [13]. One of the fascinating routes to the production of new materials with nanoporous architectures of different dimensionalities is using stable size-specific clusters as building blocks [13-20].

Zinc sulfide (ZnS) has traditionally shown remarkable fundamental properties versatility and is currently of high relevance in technological applications including light-emitting diodes (LEDs), electroluminescence, flat panel displays, infrared windows, sensors, lasers, and biodevices [21-26]. Since the transition from bulk systems to small clusters leads to substantial changes in physical and chemical properties, giving rise to unusual properties (such as the size quantization effect) that can result in promising applications, there is growing interest in the study of small clusters [27]. Up to now, ZnS clusters have been studied both theoretically and experimentally [28-48]. There is a general consensus on the lowest-energy structures for Zn_nS_n clusters based on the predictions of previous global optimizations studies: the smallest clusters

are typically planar with ring-like structures, whereas in the next range of cluster size, the dominant structural motif takes the form of spherical bubbles, where all atoms are three-coordinated. Then the onion-like structures in which one bubble is inside another become more favorable with cluster size increasing, before the dominant structural motif can be built up by cutting from bulk phases. Particularly, the structures of the smallest magic clusters of ZnS ($Zn_{12}S_{12}$ and $Zn_{16}S_{16}$) have been identified as fullerene-like [36-41, 48], perfect closed cages, or spherical bubbles, where all atoms arrange in tetragonal and hexagonal rings. Importantly, because of the octahedral character of the fullerene-like structures for these clusters, they are suitable for assembling new frameworks.

In this work, we report the results of density functional theory calculations on cluster-assembled materials based on $Zn_{12}S_{12}$ and $Zn_{16}S_{16}$, demonstrating the stability and energetic feasibility of new low-density nanoporous structures from ZnS clusters. We would firstly concentrate on the structural and electronic properties of individual $Zn_{12}S_{12}$ and $Zn_{16}S_{16}$ clusters. The pairwise interaction of the clusters will then be discussed, where we considered the plausibility of formation of particular frameworks by direct assembly of stable ZnS clusters rather than following more conventional synthetic routes. The structures, energetics, and electronic properties of the assembled-framework architectures will be subsequently discussed.

2. Computational methods

In this work, all calculations are performed using the spin-polarized density functional theory (DFT) implemented in the DMOL^3 program (Accelyrs Inc.) [49, 50]. The generalized gradient approximation formulated by Perdew, Burke, and Ernzerhof (PBE) [51] is employed to describe the exchange-correlation energy functional. Density-functional semi-core pseudopotentials (DSPPs) [52] fitted to all-electron relativistic DFT results, and double numerical basis set including d-polarization functions (i.e., the DND set) are selected. Self-consistent field (SCF) procedures are performed with a convergence criterion of 10^{-6} a.u. on the energy and electron density. The geometries are fully optimized without any symmetry constraints. We use a convergence criterion of 10^{-3} a.u. on the gradient and displacement and 10^{-5} a.u. on the total energy in geometrical optimization. Periodic boundary conditions are

employed in the solid-state calculations, and the Brillouin zone is sampled using a 3×3×3 Monkhorst-Pack [53] grid. To further explore the thermal stability of these solids, Born-Oppenheimer molecular dynamics (BOMD) is carried out in a NVT ensemble. A Nosé-Hoover chain of thermostats was used to control the temperature at 300 K. The PBE/DSPPs/DND combination is used here for BOMD. The SCF convergence criterion of 10^{-6} a.u is performed to ensure the accuracy of calculations.

3. Results and discussion

3.1 Individual $Zn_{12}S_{12}$ and $Zn_{16}S_{16}$ clusters

The lowest-energy structures of individual $Zn_{12}S_{12}$ and $Zn_{16}S_{16}$ clusters are shown in Fig. 1. $Zn_{12}S_{12}$, the smallest possible high-symmetry magic number cluster, is the first appearance of a fullerene-like cage with high symmetry (D_{2h}), which has six isolated four-membered rings (4Rs) and eight six-membered rings (6Rs) on the cluster surface. The other magic number octahedral cluster, $Zn_{16}S_{16}$, possesses six 4Rs and twelve 6Rs. It also has a high symmetry (T_d). The energy gaps between the highest-occupied molecular orbital (HOMO) and lowest-unoccupied molecular orbital (LUMO) of $Zn_{12}S_{12}$ and $Zn_{16}S_{16}$ clusters are 3.436 eV and 3.324 eV, respectively. The equilibrium geometries and electronic properties of $Zn_{12}S_{12}$ and $Zn_{16}S_{16}$ clusters we obtained are in agreement with previous theoretical studies [36-41, 48], which may confirm that the methods used in our calculations are responsibly. The octahedral configurations, high symmetries, and large HOMO-LUMO gaps demonstrate that the magic $Zn_{12}S_{12}$ and $Zn_{16}S_{16}$ clusters are particularly stable, indicating that they could be ideal building blocks to form higher order structures for synthesizing cluster-assembled materials.

3.2 Cluster-cluster interactions

In this subsection, we consider the formation of $Zn_{12}S_{12}$ and $Zn_{16}S_{16}$ dimers and their implications for forming framework materials. As shown in Fig. 1, the individual $Zn_{12}S_{12}$ and $Zn_{16}S_{16}$ clusters have two types of edges (linear Zn-S), two types of faces (4Rs and 6Rs), and two types of apexes (Zn and S atoms), respectively. Similar to the process of searching the lowest-energy structures of $Zn_{12}O_{12}$ [54] and $M_{12}N_{12}$ (M=Al, Ga) [55] dimers, in this work, we

checked all possible dimer interactions. The five lowest-energy structures of $Zn_{12}S_{12}$ dimers are shown in Fig. 2, while four lowest-energy structures of $Zn_{16}S_{16}$ dimers are shown in Fig. 3. As seen in Fig. 2 and 3, in principle there are five ways for clusters to interact with each other: (i) Joining two hexagonal-rings to form a double six-membered ring (D6R) junction, which has two types marked as D6R_1 and D6R_2. For the D6R_1 type, a 6R of one monomer is connected with a 4R of the other monomer, while for the D6R_2 type, a 6R of one monomer is connected with a 6R of the other monomer. (ii) Joining two tetragonal-rings to form a double four-membered ring (D4R) junction. (iii) Joining two edges to form four-membered ring (4R) junction, which has two types marked as 4R_1 and 4R_2. For the 4R_1 type, the 4Rs surrounding the joined edge face to 4Rs of the other monomer, and the 6Rs surrounding the joined edge face to 6Rs of the other monomer. However, for the 4R_2 type, the 4Rs surrounding the joined edge face to 6Rs of the other monomer.

For the $Zn_{12}S_{12}$ dimers, we find that the coalescence via D6R junction is the most energetically favorable [see Fig. 2(a and b)], and followed by the coalescence via D4R junction. This is very similar to the cases of other fullerene-like $X_{12}Y_{12}$ (XY=ZnO, AlN, GaN, SiC) clusters [54-56]. It is noted that the energy difference between structure a and b, which is formed by D6R_1 and D6R_2 junctions respectively, is very small (only 0.014 eV) as shown in Fig. 2. Meawhile, the binding energies per ZnS of structure a and b as shown in Fig. 2 are on the whole the same. These facts mean that both of them can be considered to be the ground state. However, for the $Zn_{16}S_{16}$ dimers, the coalescence via D4R junction is the most stable one. This is different from the case of $Zn_{16}O_{16}$ dimers. Liu and co-workers have predicted that the most stable isomer of $Zn_{16}O_{16}$ dimers is the coalescence via D6R junction [57]. The coalescence via D6R junction is 0.111 eV higher in energy than the most stable one, indicating that the coalescence on the 6R face becomes energetically unfavourable for larger clusters. This could be attributable to the elastic strain induced on the clusters when interacted with each other at 6R faces. When the 6R face coalescence is taking, the two 6Rs that form the D6R junction are arranged in parallel, which would distort the surface of the cluster [see Fig. 3(c)]. In this case, the elastic energy lost penalizing the energy that is gained from the formation of Zn-S

bonds. It should be noted that the D6R junction has only four Zn-S bonds to be formed, however, as we shall show bellow, the six Zn-S bonds of D6R junction would make contributions in cluster-assembled materials.

The strength of coalescence is quantified by the dimerization energy (E_d), which is defined by

$$E_d = E_{tot}(dimer) - 2 \times E_{tot}(monomer) \quad (1)$$

where the $E_{tot}(dimer)$ and $E_{tot}(monomer)$ are the total energies of the corresponding system. The results are summarized in Table 1. The dimerization energies are found to be negative, being indicative of the stability of these dimers. However, we note that the differences in relative energies of different junctions are much smaller (see Fig. 2 and 3), which indicates that there may be different junctions in a cluster-assembled material. Inspired by this point, we would construct cluster-assembled materials by different types of cage-cage junctions. To further analyze their relative stabilities, we also calculated the binding energy per ZnS (E_b) according to the expression

$$E_b = (nE_{Zn} + nE_S - E_{ZnS})/n \quad (2)$$

where E_{Zn} and E_S are the total energies of an isolated Zn and S atom, respectively, E_{ZnS} is the total energy of the corresponding system, and n is the number of Zn or S atoms involved. The E_b of individual $Zn_{12}S_{12}$ and $Zn_{16}S_{16}$ clusters we calculated are 5.276 eV and 5.314 eV, respectively. As the results for dimers summarized in Table 1, it is found that the E_b of dimers are always larger than the corresponding monomers, indicating that the dimers are more stable than monomers. Furthermore, the stabilities of these cluster dimers can be understood by their vibrational frequency calculations. There are no imaginary frequencies for any of them, indicating that they are located at the real minimum point of the potential energy surface.

To further discuss the assembly processes, the transition states are searched by the method of complete linear/quadratic synchronous transit (LST/ QST). The reaction paths of $Zn_{12}S_{12}$ dimers are studied, and take this an example to investigate the assembly processes. The $Zn_{12}S_{12}$ dimers as shown in Fig. 2 are viewed as products. The reactants are set as two monomers with

distances of larger 7 Å and keeping the direction of interactions between monomers unchanged (see Fig. 2). To form the dimer (shown in Fig. 2a), an energy barrier of about 0.44 eV must be overcome, conversely, the reaction to the configuration of b as shown in Fig. 2 only has to overcome a small energy barrier of about 0.08 eV. For the reactions to configurations of c, d, and e, the energy barrier is 0.37 eV, 0.12 eV, and 0.18 eV, respectively. From the kinetic prediction point of view, the reaction path clearly indicates that the interactions of two $Zn_{12}S_{12}$ monomers, the configuration of a as shown in Fig. 2 are the most favorable.

From Fig. 2 and 3, it is obvious that the structural geometries of monomers can be retained during the coalescences are occurring. Then, we consider the electronic properties of these dimers, since it is expected that some novel properties of isolated monomers would be also retained in cluster-assembled materials. The calculated HOMO-LUMO gaps of these dimers are shown in Table 1. It is found that the HOMO-LUNO gaps of dimers are very similar to that of the corresponding monomers, indicating that the basic electronic properties of monomers can be maintained in dimers.

3.3 Structural and electronic properties of cluster-assembled materials based Zn_nS_n (n=12, 16)

We now discuss the periodic systems constructed with Zn_nS_n (n=12, 16) clusters. We have considered a large number of possible initial structures of cluster-assembled materials based on Zn_nS_n (n=12, 16) clusters, in addition, we also have considered the nanoporous analogues of sodalite structures (SOD) based on Zn_nS_n (n=12, 16) clusters, which was recently proposed for nanoporous SiC, MgO, and ZnO [56-60]. The optimized stable configurations of $Zn_{12}S_{12}$- and $Zn_{16}S_{16}$-assembled frameworks are shown in Fig. 4 and 5, respectively. The junctions of each monomer, space group, lattice parameters, the volume, binding energy, and band gap of the calculated frameworks, together with wurtzite (WZ) and zinc-blende (ZB) ZnS phases, are obtained and summarized in Table 2.

For $Zn_{12}S_{12}$-assembled frameworks, we have obtained eight kinds of structures, which are shown in Fig. 4. Following the framework notation for the corresponding silicate topologies [61], it is found that structure **12-1**, **12-3**, **12-7**, and **12-8** can be viewed as SOD, LTA, FAU, and EMT phases, respectively. From the analysis of relative energies, the framework **12-1** turns

out to be the most stable one among all the frameworks considered, resembling previous studies on ZnO frameworks based on $Zn_{12}O_{12}$ clusters [54, 57, 58, 60]. It should be noted that the SOD-ZnS structure cannot be synthesized via the direct coalescence of $Zn_{12}S_{12}$ clusters, since the SOD-ZnS is formed via Zn-S edge-to-edge intercage interactions forming four-membered ring linkages. From the perspective of cluster-assembled materials, the most stable one is framework **12-3** among all the frameworks, which is formed via 6×D4R junctions [see Fig. 4(**12-3**)]. This structural framework was also investigated by Matxain *et al.* in a study on thermally stable solids based on endohedrally doped ZnS clusters [62]. Since the centers of $Zn_{12}S_{12}$ cages favor the bulk fcc structure, they predicted that the structure of the characterized solid has a cubic unit cell with lattice parameters of 13.79 Å, which corresponds to a distance of about 2.5 Å between monomers. In this work, our calculated optimum lattice parameter is found to be 13.25 Å with a distance of 2.546 Å between monomers. It is obvious that the lattice parameter we obtained is a little smaller than that of Matxain *et al.* [62]. The differences in lattice parameters may be attributed to bond lengths of the intermonomer Zn-S bonds. We found that each monomer in the structure **12-3** has two types of Zn-S bonds, a longer one (2.458 Å) in four-membered rings and the other shorter one (2.378 Å) connecting the neighboring four-membered rings, which are larger than those of isolated monomers. This feature was also found in other stable solids based on $X_{12}Y_{12}$ (XY=ZnO, AlN, GaN, and BN) clusters [54, 55, 63]. However, the bond lengths of the corresponding Zn-S bonds reported by Matxain *et al.* are 2.57 Å and 2.49 Å, respectively, which is larger than our results. Previous computational studies of cluster-assembled materials based on fullerene-like $X_{12}Y_{12}$ (XY=ZnO, AlN, and GaN) clusters have revealed that the **12-2** phases are more stable than the LTA-XY phases [54, 55]. On the contrary, in this work, the **12-2** phase [see figure 4(**12-2**)] is much less stable than the LTA-ZnS phase. It might be due to the fact that the Zn-S bond lengths between monomers are different. The average Zn-S bond length between monomers of the **12-2** ZnS phase is 2.55 Å, larger than that of their corresponding $Zn_{12}S_{12}$ dimer (2.51 Å). However, the Zn-S bond lengths between monomers of the other $Zn_{12}S_{12}$-assembled frameworks are smaller than those of corresponding $Zn_{12}S_{12}$ dimers. The increasing of bond lengths in **12-2** ZnS phase may reduce

its stability.

To check for the dynamic behavior and thermal stability of these frameworks, the first-principles Born-Oppenheimer molecular dynamics (MD) simulation was carried out for the selected case, namely, the **12-2** ZnS phase, which is less stable than others. We set a simulation time of 3 ps with a time step of 1fs, and the structural change was calculated at a constant average temperature of 300 K. Fig. 6 shows how the energies of the framework varies during the simulation. It was observed that the energy of the framework oscillates around the value (about -213215.167 eV) for the duration of the simulation, and the energy-floating ranges are no more than 0.005 eV with the simulation time increasing, a fact that is very supportive of the thermal stability of the calculated structure. This feature was found by Matxain *et al.* for other ZnS solids based on ZnS clusters [62]. Therefore, the **12-2** ZnS phase is predicted to be stable at room temperature for long enough to allow for their characterization. As mentioned above, the other $Zn_{12}S_{12}$-assembled frameworks are much more structural stability at T=0 K than the **12-2** ZnS phase. It may be predicted that the other $Zn_{12}S_{12}$-assembled frameworks are also stable at room temperature.

For $Zn_{16}S_{16}$-assembled frameworks, six kinds of frameworks are found to be stable with characterized positive frequencies. Frameworks **16-1** and **16-2** can be viewed as SOD phases, while frameworks **16-3** and **16-4** are structural analogs of zeolite LTA. For framework **16-1**, the coalescences of monomers are formed via the Zn-S edge-to-edge intercage interactions forming four-membered ring (4R) linkages (see Table 2), which is the same as the case of framework **12-1**. However, 4R and 6R linkages are found in the framework **16-2**. As seen in Fig. 5, the framework **16-3**, formed by the (4×D6R+2×D4R) junctions, is the most energetically unfavorable one because of the participation of D6R junctions, which is similar to the case of dimers for $Zn_{16}S_{16}$ clusters. Frameworks **16-5** and **16-6**, which have the 4R junctions, are more stable than frameworks **16-3** and **16-4**. Furthermore, framework **16-5** lies energetically very close to the frameworks **16-6**, suggesting that the contributions of both 4R_1 and 4R_2 junctions for the formations of different frameworks are almost degenerated in energy.

The volumes per atom of the frameworks we characterized are 15.3%~86.6% larger than that of ZB-ZnS phase, especially for the cluster-assembled phases, suggesting that these frameworks are all low-density polymorphs. For SOD-, LTA-, and FAU-MgO phases, Bromley *et al.* [58] have confirmed that their stabilities become weaker with increasing volume per atom. See Table 2, it is found the same feature for the SOD-, LTA-, and FAU-ZnS phases. However, based on an overall analysis of all the frameworks we studied, there is no direct relation between the stability and density. It can be seen from Fig. 4 and 5 that all the characterized frameworks are nanoporous materials. Due to their nanoporous structures, these frameworks based on ZnS clusters could be used in many applications such as gas storage, heterogeneous catalysis, adsorbents, and sensors [7-9].

We now investigate the electronic properties of all the predicted frameworks as shown in Fig. 4 and 5. The band structures of all the frameworks have been calculated firstly, and the direct bandgaps are potted in Table 2. Our calculations predict all the frameworks to be semiconductors with wide bandgaps. Particularly, the bandgap values of all the calculated frameworks (expect for frameworks **12-2**, **12-5**, and **12-8**) are larger than that of the ZB-ZnS phase (which is more stable than WZ-ZnS phase at room temperature). Because of the wide bandgap characteristics for these calculated frameworks, it is expected that they should be perspective materials for optoelectronic applications. As we all know, the use of GGA level of density functional theory leads to an underestimation of the one-electron band gap. For example, the calculated bandgap for WZ-ZnS phase is 2.367 eV and for ZB-ZnS phase is 2.27 eV, compared with the experimental values of about 3.77 eV and 3.72 eV, respectively. Therefore, it is predicted that the real bandgap values of all the frameworks should be similarly by about 1.4 eV higher.

To further understand the features in the band edges near the Fermi level, we also calculate the total and partial density of states (PDOS) for the frameworks based on Zn_nS_n (n=12, 16) clusters. The results of PDOS for $Zn_{12}S_{12}$- and $Zn_{16}S_{16}$-based frameworks are shown in Fig. 6 and 7, respectively. Since the cost of calculation increases rapidly with the size of unit cells, we were able to include only a limited number of the conduction states for larger unit cell materials.

Hence, there are only the lower conduction bands that are shown for some frameworks with large unit cell (e.g. frameworks **12-3** and **12-7**, i.e. LTA- and FAU-ZnS). It is found that, in general, the PDOS of all frameworks considered exhibits similar features, which could be tracked back to the atomic valence states: Zn 4s and 3d and S 3s and 3p. The valence bands near Fermi level are mainly dominated by the 3p atomic orbitals of S atoms, and the contribution of the other atomic orbitals to the valance bands is very small. The largest contribution to the conduction bands comes from the 4s orbitals of Zn atoms. Moreover, the 3d orbitals of Zn atoms and 3p orbitals of S atoms also provide partial contribution to the conduction bands.

4. Conclusions

In summary, the possibility of the formation of different low-density framework materials based on highly stable Zn_nS_n (n=12, 16) clusters is theoretically investigated using density functional theory calculations. Our cluster building blocks, which have high symmetries and large HOMO-LUMO gaps, are predicted to be strongly energetically preferred.

Dimers formed by attaching clusters on tetragonal, hexagonal, or edge (Zn-S) sites, are found to be more stable than others. The energy differences between any two dimers with different junctions are quite small, suggesting that the different junctions may coexist when the cluster assembly is formed. The characterized dimers with different junctions are further used as starting geometries. Via the coalescence of Zn_nS_n (n=12, 16) building blocks, many kinds of low-density ZnS framework materials of varying porosity are thus proposed. All frameworks differ from known synthesized materials and are energetically stable at room temperature. These new materials are found to be semiconductors with wide bandgaps, and the values of bandgaps for most of these materials are larger than that of zinc-blende ZnS phase, indicating that they may have a promise for optoelectronic applications. Because of the nanoporous character of these new materials, they could be used for gas storage, heterogeneous catalysis, and filtration and so on.

Acknowledgements

This work was supported by the National Natural Science Foundation of China (No. 11304080 and

NO.11104138).

References

[1] D. W. Breck, *Zeolite Molecular Sieves: Structure, Chemistry and Use*. (Wiley-Interscience, New York, 1974).

[2] P. B. Venuto, *Microporous Mater*., 1994, **2**, 297–411.

[3] A. Corma, *Chem. Rev.*, 1995, **95**, 559–614.

[4] D. Bradshaw, J. B. Claridge, E. J. Cussen, T. J. Prior and M. J. Rosseinsky, *Acc. Chem. Res*., 2005, **38**, 273–282.

[5] C. J. Kepert, *Chem. Commun*., 2006, 695–700.

[6] S. L. James, *Chem. Soc. Rev.*, 2003, **32**, 276–288.

[7] D. Maspoch, D. Ruiz-Molina and J. Veciana, *Chem. Soc. Rev*., 2007, **36**, 770–818.

[8] R. E. Morris and P. S.Wheatley, *Angew. Chem. Int. Ed.*, 2008, **47**, 4966–4981.

[9] J. Jiang, R. Babarao and Z. Hu, *Chem. Soc. Rev*., 2011, **40**, 3599–3612.

[10] S.T. Meek, J. A. Greathouse and M. D. Allendorf, *Adv. Mater.*, 2011, **23**, 249–267.

[11] R. Q. Snurr, *J. Phys. Chem. Lett.*, 2011, **2**, 1842–1843.

[12] B. Moulton and M. J. Zaworotko, *Chem. Rev.*, 2001, **101**, 1629–1658.

[13] S. M. Woodley and C. R. A. Catlow, *Nat. Mater.*, 2008, **7**, 937–946.

[14] S. N. Khanna and P. Jena, *Phys. Rev. Lett.*, 1992, **69**, 1664–1667.

[15] M. Qian, A. C. Reber, A. Ugrinov, N. K. Chaki, S. Mandal, H. M. Saavedra and S. N.Khanna, A. Sen, P. S. Weiss, *ACS Nano*, 2010, **4**, 235–240.

[16] S. A. Claridge, A. W. Castleman Jr., S. N. Khanna, C. B. Murray, A. Sen and P. S.Weiss, *ACS Nano*, 2009, **3**, 244–255.

[17] A. W. Castleman Jr. and S. N. Khanna, *J. Phys. Chem.C*, 2009, **113**, 2664–2675.

[18] S. Mandal, A. C. Reber, M. Qian, P. S. Weiss and S. N. Khanna, A. Sen, *Acc. Chem. Res*., 2013, **46**, 2385–2395.

[19] P. Jena, *J. Phys. Chem. Lett.*, 2013, **4**, 1432−1442.

[20] J. Kemsley, *Chem. Eng. News.*, 2013, **95**, 24−25.

[21] X. Jiang, Y. Xie, J. Lu, L. Y. Zhu and Y. T. Qian, *Chem. Mater*., 2001, **13**, 1213–1218.

[22] X. S. Fang, C. H. Ye, X. S. Peng, Y. H. Wang, Y. C. Wu and L. D. Zhang, *Adv. Funct. Mater.*, 2005, **15**, 63–68.

[23] J. Ziegler, S. Xu, E. Kucur, F. Meister, M. Batentschuk, F. Gindele and T. Nann, *Adv. Mater.,* 2008, **20**, 4068–4073.

[24] J. W. Moreau, P. K. Weber, M. C. Martin, B. Gilbert, I. D. Hutcheon and J. F. Banfield, *Science*, 2007, **316**, 1600–1603.

[25] X. S. Fang, Y. Bando, M. Y. Liao, U. K. Gautam, C. Y. Zhi, B. Dierre, B. D. Liu, T. Y. Zhai, T. Sekiguchi, Y. Koide and D. Golberg, *Adv. Mater.*, 2009, **21**, 2034–2039.

[26] X. S. Fang, Y. Bando, U. K. Gautam, C. H. Ye and D. Golberg, *J. Mater. Chem.*, 2008, **18**, 509–522.

[27] F. Baletto and R. Ferrando, *Rev. Mod. Phys*., 2005, **77**, 371–423.

[28] A. Mohajeri and M. Alipour, *Int. J. Quantum. Chem*., 2011, **111**, 3841–3850.

[29] J. M. Matxain, J. E. Fowler and J. M. Ugalde, *Phys. Rev. A*, 2000, **61**, 053201.

[30] J. M. Azpiroz, E. Mosconi and F. D.Angelis, *J. Phys. Chem. C*, 2011, **115**, 25219–25226.

[31] S. Hamad, C. R. A. Catlow, E. Spano, J. M. Matxain and J. M.Ugalde, *J. Phys. Chem. B*, 2005, **109**, 2703–2709.

[32] S. Pal, B. Goswami and P. Sarkar, *J. Phys. Chem. C* 2008, 112, 6307–6312.

[33] S. Hamad and C. R. A. Catlow, *J. Cryst. Growth*, 2006, **294**, 2–8.

[34] S. Pal, R.Sharma, B. Goswami, P. Sarkar and S. P. Bhattacharyya, *J. Chem. Phys.*, 2009, **130**, 214703.

[35] E. Spanó, S. Hamad and C. R. A. Catlow, *Chem. Commun.*, 2004, 864–865.

[36] K. Chuchev and J. J. BelBruno, *J. Phys. Chem. A*, 2005, **109**, 1564–1569.

[37] S. Pal, B. Goswami and P. Sarkar, *J. Chem. Phys.*, 2005, **123**, 044311.

[38] C. R. A. Catlow, S. T. Bromley, S. Hamad, M. Mora-Fonz, A. A. Sokola and S. M. Woodley, *Phys. Chem. Chem. Phys.*, 2010, **12**, 786–811.

[39] E. Spanó, S. Hamad and C. R. A. Catlow, *J. Phys. Chem. B*, 2003, **107**, 10337–10340.

[40] X. Zhang, M. Zhao, T. He, W. Li, X. Lin, Z. Wang, Z. Xi, X. Liu and Y. Xia, *Solid State Commun*., 2008, **147**, 165–168.

[41] S. Hamad, S. M. Woodley and C. R. A.Catlow, *Molecular Simulation*, 2009, **35**, 1015–1032.

[42] A. Burnin, E. Sanville and J. J. BelBruno, *J. Phys. Chem. A*, 2005, **109**, 5026–5034.

[43] A. Burnin and J. J.BelBruno, *Chem. Phys. Lett.*, 2002, **362**, 341–348.

[44] A. Mohajeri, M. Alipour and M. B. Ahmadi, *Chem. Phys. Lett.*, 2011, **503**, 162–166.

[45] H. Chen, D. Shi, B. Wang and J. Qi, *J. Comput. Theor. Nanos*., 2011, **8**, 2454-2461.

[46] G. Malloci, L. Chiodo, A. Rubio and A. Mattoni, *J. Phys. Chem. C*, 2012, **116**, 8741–8746.

[47] D. L. Lalsare and A. Kshirsagar, *Bull. Mater. Sci.*, 2012, **35**, 1055–1062.

[48] K. A. Nguyen, R. Pachter and P. N. Day, *J. Chem. Theory Comput.*, 2013, **9***, 3581–3596.*

[49] B. Delley, *J. Chem. Phys.*, 1990, **92**, 508–517.

[50] B. Delley, *J. Chem. Phys.*, 2000, **113**, 7756–7764.

[51] J. P. Perdew, K. Burke and M. Ernzerhof, *Phys. Rev. Lett.*, 1996, **77**, 3865–3868.

[52] D. R. Hamann, M. Schluter, C. Chiang, *Phys. Rev. Lett.*, 1979, **43**, 1494–1497.

[53] K. J. Monkhorst and J. D. Pack, *Phys. Rev. B*, 1976, **13**, 5188–5192.

[54] Y. L. Yong, B. Song and P. He, *J. Phys. Chem. C*, 2011, **115***,* 6455–6461.

[55] Y. L. Yong, B. Song and P. He, *Phys. Chem. Chem. Phys.*, 2011, **13**, 16182–16189.

[56] M. B. Watkins, S. A. Shevlin, A. A. Sokol, B. Slater, C. R. A. Catlow and S. M.Woodley, *Phys. Chem. Chem. Phys.*, 2009, **11**, 3186–3200.

[57] Z. Liu, X. Wang, J. Cai, G. Liu, P. Zhou, K. Wang and H. Zhu, *J. Phys. Chem. C*, 2013, **117**, 17633−17643.

[58] J. Carrasco, F. Illas and S. T. Bromley, *Phys. Rev. Lett.*, 2007, **99**, 235502.

[59] M. A. Zwijnenburg, F. Illas and S. T. Bromley, *Phys. Rev. Lett.*, 2010, **104**, 175503.

[60] S. M. Woodley, M. B. Watkins, A. A. Sokol, S. A. Shevlin and C. R. A. Catlow, *Phys. Chem. Chem. Phys.*, 2009, **11**, 3176–3185.

[61] S. M. Auerbach, K. A. Carrado, P. K. Dutta, *Handbook of zeolite science and technology.* (Marcel Dekker, Inc., New York, 2003).

[62] J. M. Matxain, M. Piris, X. Lopez and J. M. Ugalde, *Chem. Eur. J*., 2009, **15**, 5138–5144.

[63] J. M. Matxain, L. A. Eriksson, J. M. Mercero, X. Lopez, M. Piris, J. M. Ugalde, J. Poater, E. Matito and M. Sola, *J. Phys. Chem. C*, 2007, **111**, 13354–13360.

Table 1. Binding energy per ZnS (E_b), dimerization energy (E_d), and HOMO–LUMO gap (E_g) of the lowest-energy structures of Zn_nS_n (n=12, 16) dimers.

species	isomers	E_b (eV)	E_d (eV)	E_g (eV)
$Zn_{12}S_{12}$ dimers	a	5.3113	-0.845	3.150
	b	5.3107	-0.831	3.214
	c	5.308	-0.771	2.296
	d	5.302	-0.613	3.343
	e	5.300	-0.579	3.395
$Zn_{16}S_{16}$ dimers	a	5.345	-0.979	3.202
	b	5.345	-0.975	3.213
	c	5.341	-0.869	3.119
	d	5.335	-0.660	3.224

Table 2. The junctions of each monomer (*junction*), space group (*S*), lattice constants, the volume per ZnS unit (*V*), the binding energy per ZnS (E_b), and the band gap (E_g) for the calculated frameworks together with WZ and ZB phases.

system	*Junction* [a]	*S*	*lattice constants*			V (Å^3)	E_b (eV)	E_g (eV)
			a(Å)	b (Å)	c (Å)			
WZ		P63MC	3.823	3.823	6.261	39.624	5.831	2.367
ZB		F-43M	5.420	5.420	5.420	39.805	5.842	2.270
12-1	$4R^6$	PM-3N	6.552	6.552	6.552	46.880	5.559	2.820
12-2	$D6R\_1^8$	R-3	8.135	8.135	8.135	39.895	5.129	1.959
12-3	$D4R^6$	FM-3C	13.250	13.250	13.250	68.533	5.477	2.993
12-4	$D4R^2$+$4R\_1^4$	P2/C	9.070	9.070	17.110	58.648	5.301	2.390
12-5	$4R\_1^4$+$4R\_2^2$	P-1	9.050	9.050	9.170	59.752	5.352	2.240
12-6	$D6R\_1^2$+$4R\_1^2$+$4R\_2^2$	P-1	7.754	9.178	9.178	52.920	5.396	2.558
12-7	$D6R\_1^4$	FD-3	18.89	18.89	18.89	70.214	5.416	2.530
12-8	$D6R\_1^2$+	P-31C	14.000	14.000	21.000	74.259	5.373	2.150
16-1	$4R^6$	CMM2	22.039	22.039	15.584	47.309	5.408	2.395
16-2	$6R^4$+$4R^2$	P-1	6.864	6.864	15.584	45.890	5.451	2.440
16-3	$D6R^4$+$D4R^2$	P4/NBM	13.152	13.152	9.865	53.326	5.298	2.440
16-4	$D4R^6$	P-43M	9.865	9.865	9.865	60.003	5.357	2.721
16-5	$D4R^4$+$4R\_2^2$	P2/C	9.900	9.900	23.823	62.347	5.418	2.531
16-6	$D4R^2$+$4R\_1^2$+4	P-4	20.787	20.787	9.865	66.604	5.430	2.776

[a]Notations: e.g. $D4R^2$+$4R\_1^2$+$4R\_2^2$ represent there are two D4Rs, two 4R_1s, and two 4R_2 junctions for one monomer in the corresponding framework.

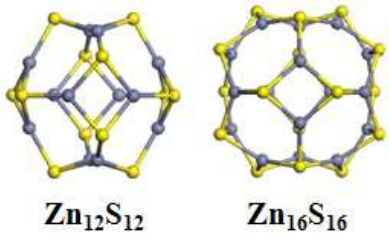

Fig.1. The optimized structures of $Zn_{12}S_{12}$ and $Zn_{16}S_{16}$ clusters. Here and in the following figures, Zn atoms are gray, and S atoms are yellow.

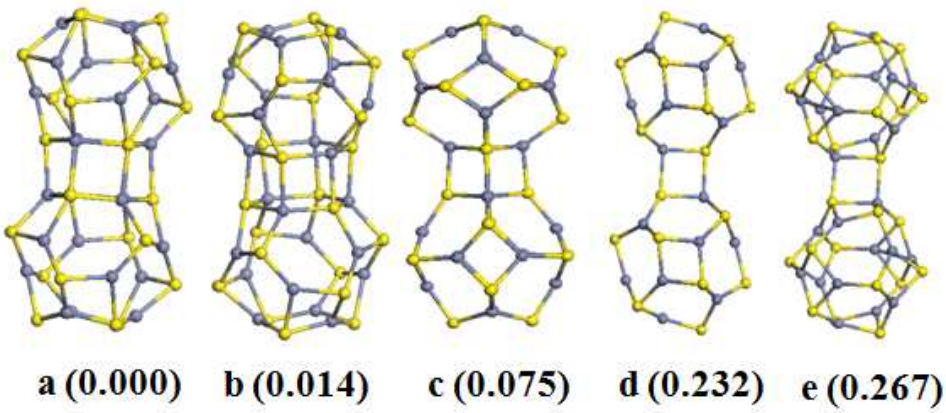

Fig. 2. Five lowest-energy structures of $Zn_{12}S_{12}$ cluster dimers, where (a) shows a D6R_1 junction, (b) shows a D6R_2 junction, (c) shows a D4R junction, (d) shows a 4R_1 junction, and (e) shows a 4R_2 junction. Values in parentheses are relative energies.

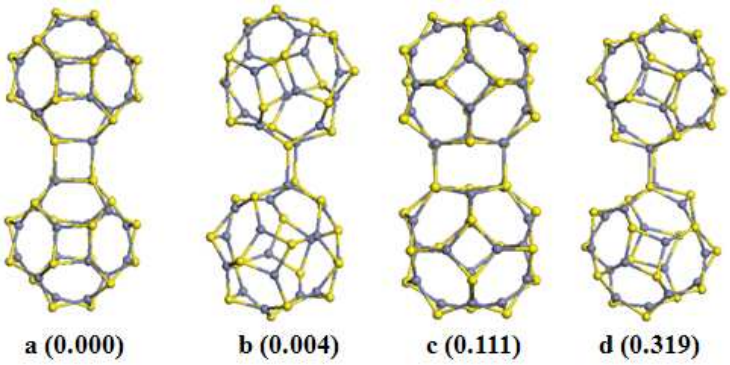

Fig. 3. Five lowest-energy structures of $Zn_{16}S_{16}$ cluster dimers, where (a) shows a D4R junction, (b) shows a 4R_1 junction, (c) shows a D6R junction, and (d) shows a 4R_2 junction. Values in parentheses are relative energies.

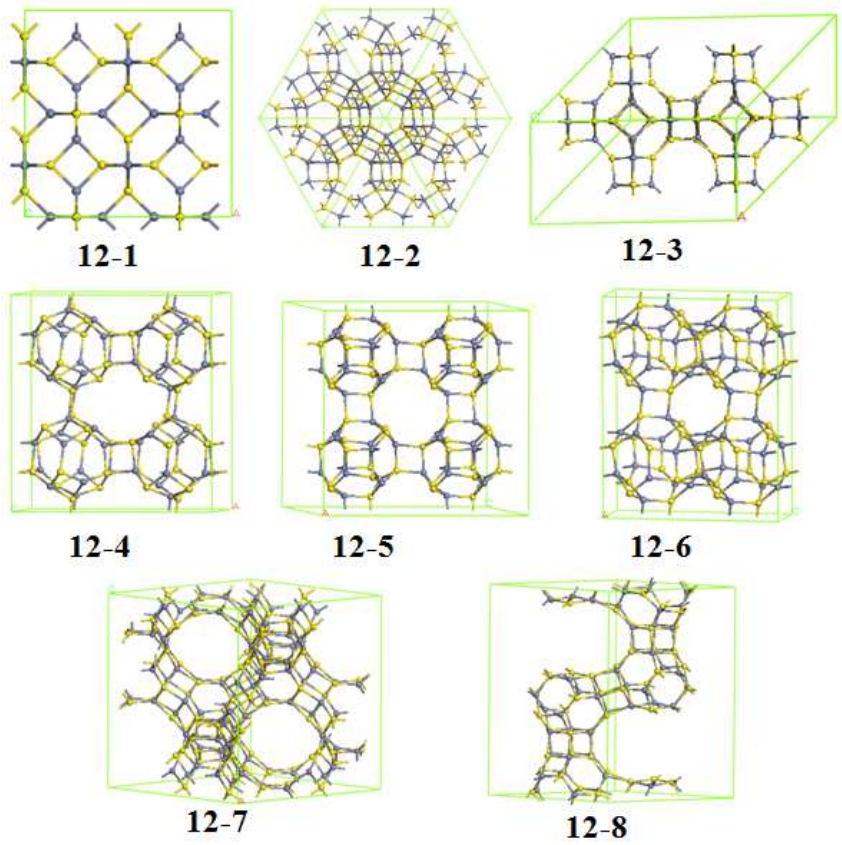

Fig. 4. The optimized stable structures of frameworks assembled by $Zn_{12}S_{12}$ clusters.

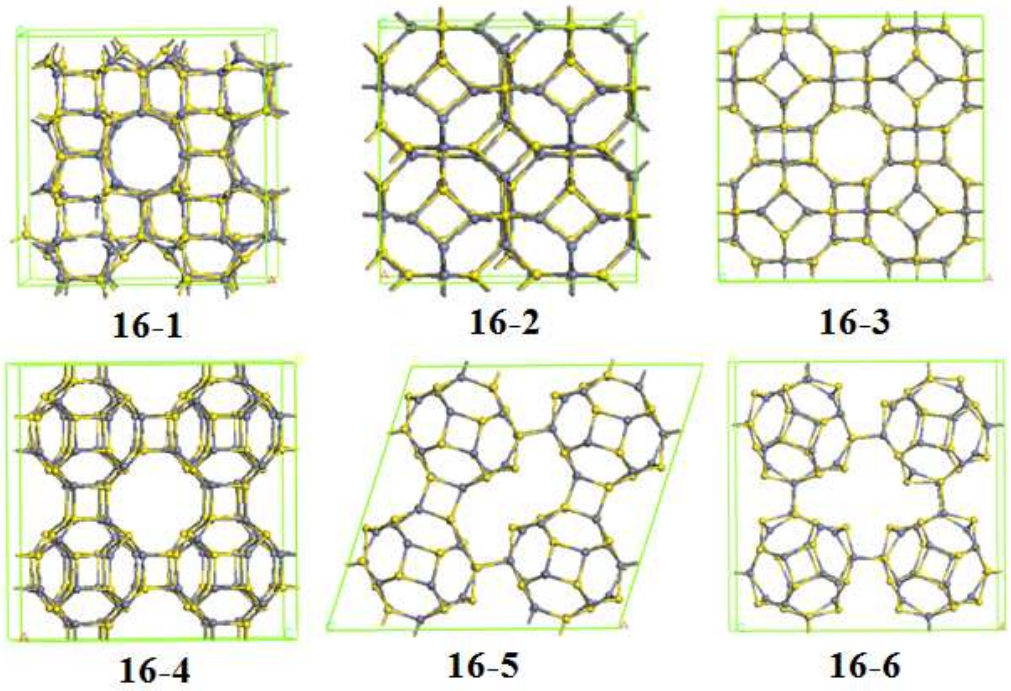

Fig. 5. The optimized stable structures of frameworks assembled by $Zn_{16}S_{16}$ clusters.

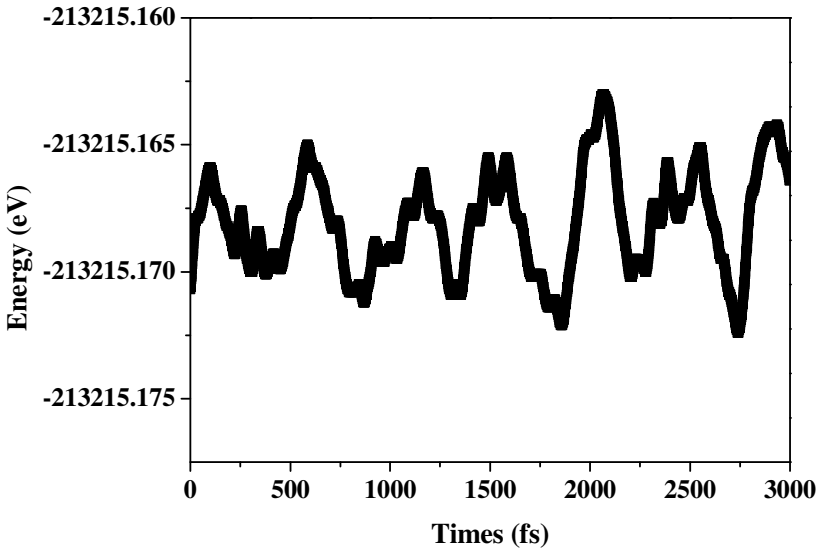

Fig. 6. Variation in the energy (eV) of the **12-2** ZnS phase (as shown in figure 4(**12-2**)) as a function of time.

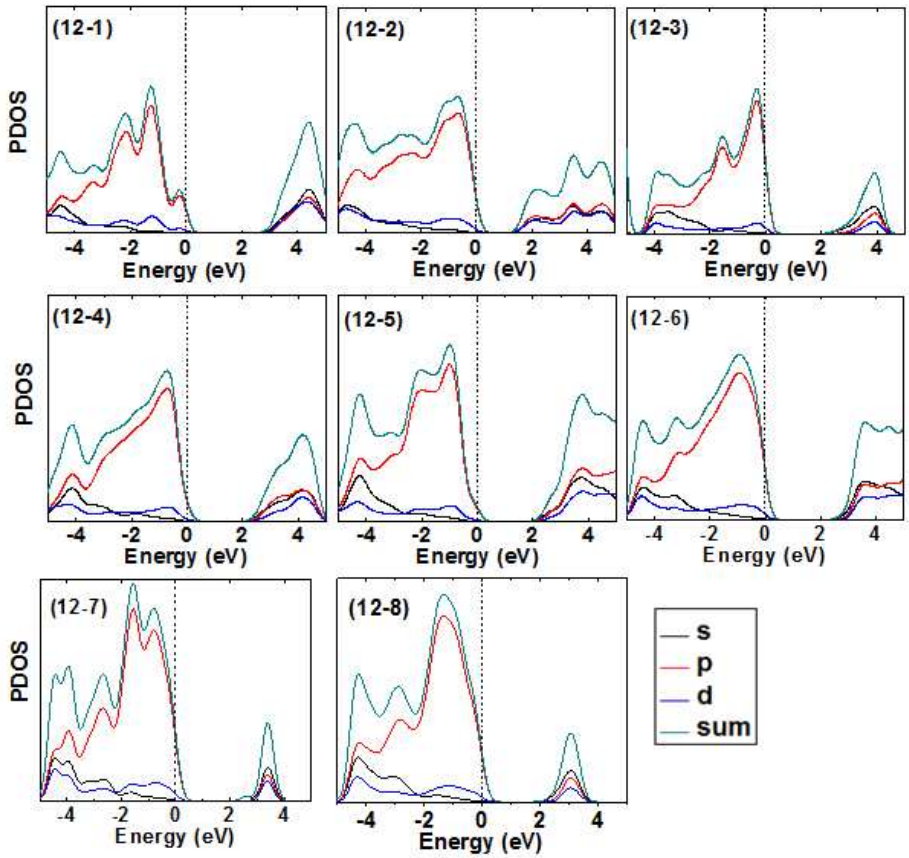

Fig. 7. Total and partial density of states for the $Zn_{12}S_{12}$-based frameworks. The vertical line indicates the Fermi level.

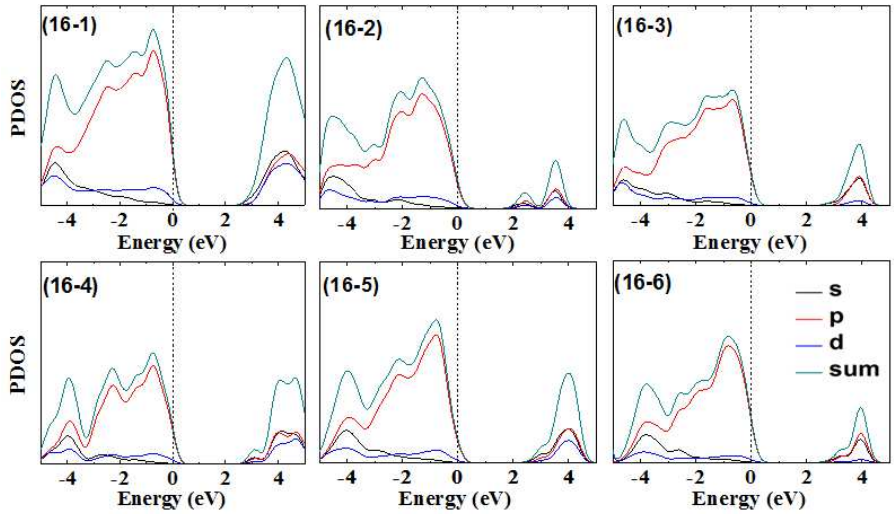

Fig. 8. Total and partial density of states for the $Zn_{16}S_{16}$-based frameworks. The vertical line indicates the Fermi level.